Magnetostriction of field-structured magnetoelastomers

James E. Martin,[1] Robert A. Anderson,[1] Douglas Read,[1] and Gerald Gulley[2]
[1]*Sandia National Laboratories, Albuquerque, New Mexico 87185, USA*
[2]*Dominican University, River Forest, Illinois 60305, USA*
(Received 28 September 2005; published 22 November 2006)

We investigate the magnetostriction of field-structured magnetoelastomers, which are an important class of materials that have great potential as both sensors and actuators. Field-structured magnetoelastomers are synthesized by suspending magnetic particles in a polymeric resin and subjecting these to magnetic structuring fields during polymerization. These structuring fields can consist of as many as three orthogonal ac components, allowing a wide variety of particles structures—chains, sheets, or networks—to be formed. A principal issue is how particle structure and loading affects the magnetostriction of these materials. To investigate magnetostriction in these field-structured composites we have constructed a constant stress, optical cantilever apparatus capable of 1 ppm strain resolution. Magnetoelastomers having a wide range of particle loadings and structures are investigated, and it is shown that the observed deformation depends strongly on composite structure. The best magnetoelastomers exhibit a contractive strain of 10 000 ppm, the worst materials exhibit a negative, tensile response, which we show is due to the dominance of demagnetizing field effects over magnetostriction. Finally, some discussion is given to the surprising finding that magnetostriction is proportional to the sample prestrain. Simulations of a chain of particles in an elastomer show that particle clumping transitions can occur, but this does not account for the dependence of magnetostriction on prestrain.

DOI: 10.1103/PhysRevE.74.051507 PACS number(s): 83.80.Gv, 75.80.+q

I. INTRODUCTION

There is a need for soft actuators that have a much larger strain response than piezoelectrics, and that can generate stress in microseconds. To this end we are developing efficient field-structured magnetostrictive elastomers (FSMEs) [1–4]. FSMEs are synthesized by first dispersing magnetic particles in a prepolymer resin. Multidimensional ac magnetic fields are then used to organize the particles into complex structures during polymerization. A wide variety of structures can be produced, including particle chains, sheets, networks, honeycombs, etc. [5]. These structures have very different magnetization behaviors, with the best composites having a specific susceptibility a decade larger than the worst [6,7]. Because magnetostriction depends quadratically on composite susceptibility [8], the method of field structuring should be an important method of controlling the response of these materials. The goal of this paper is to understand the relationship between structure and magnetostriction, and to use this to develop magnetoelastomers that have an optimal response.

In this paper we first describe the theory of magnetostriction, the synthesis and processing of FSMEs, and the optical cantilever apparatus used to measure the material strain. A discussion of how to correct the observed material strain response for the opposing effect of demagnetizing fields is given, and it is shown that the demagnetizing field stress can dominate the magnetostrictive stress for some materials. The observed extraordinary response of certain FSMEs is reported, and is demonstrated to be a result of the strong negative susceptibility anisotropy of these particular materials. We then show that the magnetostriction data for a variety of materials conform to the predictions of theory: FSMEs made of particle chains exhibit very large magnetostriction when the field is applied parallel to the chains; FSMEs made of particle sheets exhibit a very small response when the field is applied normal to the sheets; and FSMEs structured with heterodyned triaxial fields exhibit the largest magnetostriction of all.

Finally, some discussion is given of the surprising discovery that the observed magnetostriction actually increases with sample prestrain. In an attempt to explain this observation, simulations are given of a chain of magnetic particles subjected to a uniform field. It is found that the applied field can cause a hierarchy of particle clumping transitions, which occur at a set of critical fields. These transitions are shown to be hysteretic, in the sense that the declumping transitions occur at lower fields than the corresponding clumping transitions.

II. THEORY OF MAGNETOSTRICTION

A. Deformations in an initially uniform magnetic field.

When a magnetic particle composite is placed in an initially uniform magnetic field it may deform for a number of reasons. First, the individual particles can exhibit magnetostriction, causing a macroscopic deformation of the sample. This mechanism is negligible at the ~0.1 T fields we apply to our samples, and even if the applied field did create appreciable stresses in the stiff ferrous particles, these would not appreciably transmit through the soft polymer matrix. Second, dipolar interactions between particles can cause magnetostriction of the sample. This is the effect we wish to isolate. Third, sample shape can create demagnetizing fields [9] that can cause significant deformation. This is an effect we try to minimize in our experiments, but can still be the dominant effect for some samples [10]. Fourth, if ferrous pole pieces are used to direct the flux lines to the sample it is possible for image interactions to occur from the capping

magnetic monopoles. This is not a factor in our apparatus, but has probably contributed to reports of "negative magnetostriction" in particle composites. Fifth, under special circumstances the field can exert a body torque on the sample, even when the field lines are directed along the major axis of the sample. This torque can lead to large measured strains in our apparatus, but only for samples synthesized to minimize magnetostriction. Rather than embark on a full analysis of all of these effects at this point, we have chosen to describe each of these as needed to interpret our experimental results.

B. Magnetostriction

Magnetostriction is a result of the tendency of the magnetized particles to move in such a way as to increase their magnetic moments. The typical tendency is for dipole pairs aligned with the applied field to approach each other, causing a contraction of the sample along the field, and dipole pairs perpendicular to the field to push each other away, reinforcing the contraction along the field, due to the fact that the Poisson ratio is close to 1/2 for these materials.

C. Self-consistent point dipole theory

In a recent theoretical paper it has been shown that composites of magnetizable particles in an elastic continuum have the potential to exhibit large magnetostrictive stresses and strains, provided the particles can be suitably arranged [8]. This paper treats composites that have *at most* one unique axis, taken to be the z axis, along which the field is applied. For example, a composite consisting of chains formed by a uniaxial structuring field will have its unique axis parallel to the chains. A composite structured into sheets by a biaxial field (see below) will have its unique axis normal to the sheets, and a composite structured by a triaxial field (below) may not have a unique axis, nor will a random composite. The goal of this paper is to predict the stresses that the field will induce in the composite in the directions parallel and perpendicular to the applied field. The principal conclusion is that it is possible to use fields to create particle composites that have significantly enhanced or suppressed magnetostriction relative to random particle composites.

Because this theoretical paper has motivated the experimental work described herein, it is helpful to give the predictions. We do so in terms of magnetic variables, though the original paper is written in the language of electrostatics. The case of magnetostriction is slightly simpler, because the susceptibility of the continuous, polymer phase will normally be very close to zero, and thus the permeability of the polymer phase will be nearly that of free space, μ_0.

In the self-consistent local field approximation the magnetostrictive stresses parallel (z axis) and perpendicular (x axis) to the applied field are

$$\sigma_z = -\frac{1}{2}\mu_{eff}\mu_0 H_0^2(1+\gamma_{zz}),$$

$$\sigma_x = +\frac{1}{2}\mu_{eff}\mu_0 H_0^2(1-\gamma_{zx}). \tag{1}$$

Here μ_{eff} is the effective *relative* composite permeability (dimensionless) $\mu_{eff}=[1+2\beta(\phi+\psi_2)]/[1-\beta(\phi-2\psi_2)]$, which depends on the relative particle permeability μ_p through the contrast factor $\beta=(\mu_p-1)/(\mu_p+2)$, and depends on the composite structure through the parameter ψ_2 discussed below, and the particle volume fraction ϕ. The magnetostriction coefficients are defined by the strain derivatives $\gamma_{zi}=-\mu_{eff}^{-1}\partial\mu_{eff,z}/\partial s_i$, $i=x,y,z$. A calculation gives

$$\gamma_{zi}=\frac{(\mu_{eff}-1)(\mu_{eff}+2)}{3\mu_{eff}}-\lambda_i\frac{(\mu_{eff}-1)^2}{\mu_{eff}}, \tag{2}$$

where $\lambda_z=\frac{-2}{\pi\sqrt{3}}+\frac{2}{7}\frac{(3\psi_2-\psi_4)}{\phi}$ and $\lambda_x=\frac{1}{\pi\sqrt{3}}+\frac{4}{7}\frac{(3\psi_2-\psi_4)}{\phi}$. An incompressible composite will have Poisson ratio of 1/2, so a field-induced compression along the z axis must be accompanied by a volume conserving expansion in the x,y directions. The measured stress will thus be $\sigma_{meas}=\sigma_z-\sigma_x$.

Magnetostriction of particle composites depends on the structural parameters ψ_2 and ψ_4, and is notably independent of the particle size. These parameters are given in terms of the kth Legendre polynomial $P_k(x)$ by

$$\psi_k=-\sum_{j\neq i}\left(\frac{a}{r_{ij}}\right)^3 P_k(\cos\theta_{ij}), \tag{3}$$

where r_{ij} is the distance between a pair of particles in the composite, and θ_{ij} is the angle of their line of centers to the direction of the applied field. These sums are taken over a spherical cavity centered on the ith particle, then averaged over a statistical number of particles.

D. Predictions for simulated structures

To evaluate these structural parameters we must have a model of structure. We have developed a Brownian dynamics simulation that enables us to model structure in one- (1D), two- (2D), and three-dimensional (3D) fields for composites containing 10 000 particles. A detailed description of these simulations and the predicted magnetostriction coefficients can be found in Refs. [5,8].

From these simulated structures we have obtained the structural parameters for composites formed in uniaxial and biaxial fields, as well as for random composites. In the reduced stress units, $\sigma'_{meas}=\sigma_{meas}/\frac{1}{2}\mu_{eff}\mu_0 H_0^2$, where the stress is normalized by the energy density of the field, we have predicted that the reduced stress of a random 10 vol. % composite should be −2.7, the minus sign denoting a compressive stress. For a uniaxial composite the reduced stress is enhanced several fold, −6.9, whereas for a biaxial composite with the field directed normal to the sheets the reduced stress is slightly suppressed, −2.5. At higher particle loadings the stresses are larger, but the predicted trends are similar. The maximum stress we computed was for the magnetic ground state structure, the body center tetragonal lattice. A 10 vol. % composite containing aligned body-centered tetragonal (bct) domains would have a reduced stress of −9.4.

Unfortunately, it is not possible for us to make magnetostriction predictions for samples structured in triaxial magnetic fields, because the mean-field approximation of our magnetostriction theory becomes poor in this case. In es-

sence, the mean field theory predicts that the sum of the inverse composite susceptibilities taken along three principal directions is invariant to structuring [6]. Triaxial composites violate this sum rule, due to the pure many-body nature of the interactions in this case. We have discussed this point in detail elsewhere [7].

III. SYNTHESIS AND PROCESSING

A. Motivation

The goal of synthesis is to produce materials with optimal magnetostriction. As the above theoretical discussion indicates, this is roughly equivalent to finding a method of *athermally* organizing the dense, micron-size particles into structures that maximize their effective permeability. The innovation of triaxial magnetic field structuring has made the optimization of athermal composites possible, and we have described synthesis in triaxial magnetic fields in detail elsewhere [7]. Here we would only like to give a brief description of the synthesis methods we have used, the motivation for using these, and the resulting susceptibility enhancements achieved.

B. Materials

The magnetostrictive coefficient is independent of particle size, provided this is much larger than a single magnetic domain, typically tens of nanometers. Multidomain particles can be magnetically "soft," meaning the remanent magnetization is negligible, or "hard," meaning the remanence is significant, such as in permanent magnet materials. We prefer to use soft magnetic particles, as these eliminate remanent strain.

The susceptibility of the material of which the particles are made is not terribly important. When a field is applied to a soft magnetic particle the resultant magnetization is the product of the particle susceptibility times the field. One might assume the particle susceptibility is equal to the susceptibility of the material of which it is composed, but this is only true when the material susceptibility is quite small—too small to be of interest here. In fact, the particle susceptibility is practically independent of the material susceptibility and is mostly a function of the particle shape. Material susceptibilities are commonly in the range of 10^2-10^5 but the susceptibility of a sphere is limited to 3 (MKS) [11], because its magnetization creates a demagnetizing field that opposes the applied field. Thus high susceptibility materials are of no obvious benefit.

To achieve large magnetostriction the saturation magnetization of the particles should be as large as possible. FSMEs contain nearly contacting particles aligned with the applied field. In the particle gaps the fields can become exceedingly large (~100x the applied field) causing magnetic saturation of the proximal parts of the particles, which limits their mutual attraction. To avoid this it is desirable to choose particles with high saturation magnetization, such as Fe, which has a moment of ~2.2 Bohr magnetons per atom, giving a saturation magnetization of 2.1 T. (Fe also has little remanence.) We use 3–5 micron carbonyl iron particles, obtained from Lord Corporation, curing these in the silicone polymer, Gelest Optical Encapsulant 41. To minimize demagnetizing field effects, the samples are cast as long solid rectangles, of dimensions $3.25\times3.25\times50.0$ mm, unless otherwise specified.

C. Using magnetic fields to create structure

More than merely being a practical approach, magnetic fields are an ideal way of creating structure, since they naturally lead to structures that optimize the composite permeability in a carefully annealed thermal system—one in which particle diffusion insures that a free energy minimum is attained in the applied field. This is an obvious point: in an applied field the ground state particle structure is that which minimizes the net magnetostatic energy, and at low fields this energy is negative and proportional to the composite effective susceptibility. The suspension will therefore evolve to maximize its permeability, and so it would seem that a simple uniaxial magnetic field would be optimal for structuring particle composites.

Composites with such *annealed disorder* are not practically achievable in the laboratory, because this would require that the dipolar interactions generate particle forces comparable to the thermal fluctuations that give rise to diffusion. If the applied field is turned down so as to achieve this condition, the particles will simply sediment. To eliminate the effect of gravity, significant fields must be used (0.01–0.02 T). In such fields the dipolar interactions completely dominate thermal fluctuations, so the structures that form are an example of *quenched disorder*. We have shown that *heterodyned* triaxial magnetic fields can be used to create structures with quenched disorder that mimic those having annealed disorder, and have demonstrated through permeability measurements that composites structured by heterodyning have optimized magnetic properties [7].

D. Field structuring

The FSMEs investigated in this paper were made by exposing a suspension of 3–5 μm Fe or 4–7 μm Ni particles in a silicone to magnetic fields while the resin gels. The samples are then post cured at 70 °C for 4 h. The structuring fields are created by a resonant triaxial Helmholtz coil of our own design. This computer-controlled magnet and its associated tunable fractal capacitor bank are described elsewhere [7].

A variety of structures can be created by dynamic magnetic fields. A uniaxial magnetic field, created by a Helmholtz coil or by two parallel plate magnets, causes the particles to form chains. But a biaxial field, created by applying two orthogonal ac fields, leads to layered composite consisting of particle sheets in the field plane. Finally, a triaxial magnetic field can be created by combining three orthogonal magnetic fields, at least two of which are ac. Composites formed in triaxial fields can have a variety of structures, and some of these have highly optimized magnetic properties, so a brief discussion of this is worthwhile.

E. Triaxial fields

Particle interactions in triaxial fields are complicated [5], but a qualitative discussion will help understand their effects. The magnetic interactions between vicinal particles are largely due to their dipole moments, provided their gap is of order 10% of the particle diameter. At low fields the dipole moment is proportional to the local field, which is comprised of two contributions: the applied field and the field due to all the other dipoles. In a *balanced* triaxial field (i.e., all rms field component amplitudes equal) the time-average interaction between the moments induced by the applied field is zero, so the only nonvanishing interaction is due to the fields produced by the other dipoles. Thus the interaction is solely due to many-body effects, so that the interaction between any two particles is strongly dependent on the positions of the other particle. Pairwise additivity of these interactions is not even a useful first approximation.

A triaxial field has three components, each of which has an amplitude and frequency, for a total of six parameters. In a balanced triaxial field the root-mean-square (rms) amplitudes are equal, which reduces the field parameters to four. Within reasonable limits the field amplitude only determines the time scale of particle motions, and because this is not germane to the structures produced, we really only have to worry about the three field frequencies. At reasonably high field frequencies (>100 Hz), it is only the beat frequencies between the fields that are important, and there are only two such difference frequencies, and thus only two parameters.

The beat frequencies between the field components can have a significant effect on composite structure when they are low enough that the prepolymer/particle suspension can follow the beats. We will use the term triaxial field to refer to the case where the two beat frequencies are so large (greater than ~ 25 Hz) that the particle suspension cannot follow the beats. This leads to isotropic networks of particle chains. The term 2D heterodyning will refer to the case where the particle suspension can follow only one beat frequency (e.g., component frequencies of 0 Hz, 200 Hz, 201 Hz), and results in an anisotropic honeycomb structure. 3D heterodyning will refer to the case where the suspension can follow both beat frequencies (e.g., 200 Hz, 201 Hz, 202 Hz). This results in an isotropic particle foam structure.

F. Composite susceptibilities

An interesting aspect of magnetic particle composites that is not always fully appreciated is just how small their susceptibilities are compared to that of the material of which their constituent particles are composed. One sometimes sees a sort of "rule of mixing" assumption, where the susceptibility of the composite is taken to be the product of the volume fraction of the particle phase times the susceptibility of the material of which the particles are made, but in fact this assumption can be very poor, because the susceptibility of a single particle is much more a function of the shape and orientation of the particle than of the material of which it is composed. For example, the susceptibility of a spherical particle is just $\chi_p = 3\beta = 3(\mu_p - 1)/(\mu_p + 2)$. For a material of high relative permeability μ_p, such as Fe or Ni, the particle susceptibility approaches 3. The Maxwell-Garnet prediction for the susceptibility of a *random* composite is then just $\chi_{eff} = 3\phi/(1-\phi)$. For small volume fractions this gives a specific susceptibility χ_{eff}/ϕ close to 3. This specific susceptibility can be thought of as the effective susceptibility of a typical particle entrained in the composite.

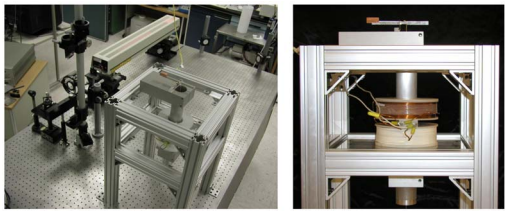

FIG. 1. (Color online) (left) Overview of the optical cantilever apparatus. (right) Side view of the cantilever and the Helmholtz coil. The coil is elevated above the stainless steel table to reduce the magnetic image of the Helmholtz coil.

The effectiveness of field structuring has been quantified from measurements on Ni particle samples made at a loading of $\phi = 6.8$ vol. % [7]. A random composite gave a specific susceptibility $\chi_{eff}/\phi = 7.1$, which exceeds the Maxwell-Garnet prediction of ~ 3 because the particles are not spherical. A composite structured by a uniaxial magnetic field was found to have a specific susceptibility of 17.2 along the structuring field (defined as the z axis) and 5.7 in the x-y plane normal to this. A composite structured with a biaxial field in the x-y plane gave $\chi_{eff}/\phi = 4.9$ along the z axis, and 14.7 in the field plane. Finally, a composite formed in a 3D heterodyned field with the z-axis field component biased by +25% gave $\chi_{eff}/\phi = 23.1$ along the z axis and 10.3 normal to this. Biased heterodyning thus enables the formation of anisotropic composites whose susceptibilties significantly exceed those created by a simple unaxial field, and should therefore have much greater magnetostriction.

IV. MAGNETOSTRICTION MEASUREMENTS

A. Optical cantilever apparatus

The reduction of demagnetizing fields is a principal difficulty in designing an apparatus to measure magnetostriction. These fields are created by the magnetization of the sample itself and oppose the applied field, seriously reducing the field in the sample. The magnitude of demagnetizing fields is strongly dependent on the shape of the magnetic sample. In order for the applied field to penetrate the sample the field must be applied along a long axis of the solid, e.g., in the plane of a sheet or parallel to a long cylinder. An optical cantilever apparatus readily accommodates long thin samples, and enables the samples to be prestressed, which is important to the magnitude of the effect. In the completed apparatus, Fig. 1, the magnetoelastomer is suspended from a cantilever, centered in a Helmholtz coil, and prestressed by adding weights to the cantilever. Strain measurements are thus made at constant stress. A mirror on the cantilever deflects a laser beam, which hits a 640×480 CCD array after a 6 m beam path. A small beam spot is created by imaging, with a simple lens, a 50 μm aperture positioned a few cm in

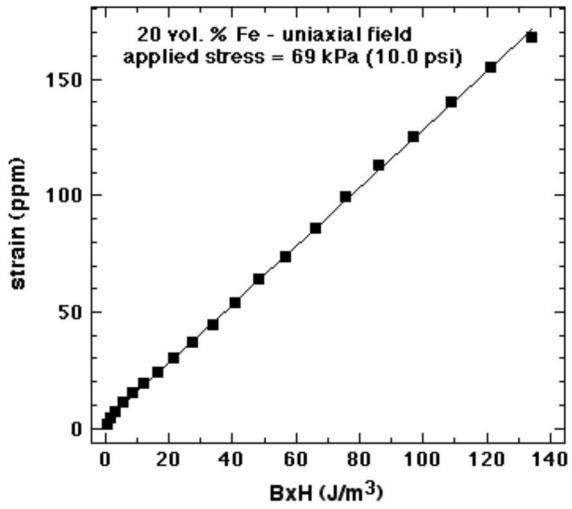

FIG. 2. Experiments at low fields show the strain is proportional to the energy density of the field. These data are for a 20 vol. % sample structured by a uniaxial magnetic field.

front of the He-Ne laser onto the CCD. This apparatus has ~50 nm displacement resolution, which for a 50 mm sample is ~1 ppm strain resolution.

The Helmholtz coil was designed for high field homogeneity and low power dissipation. Field homogeneity was optimized by a careful selection of the coil spacing, and power dissipation was minimized by making the coil cross section as thick as practical. The coil pair resistance is 2.2 Ohm and each coil is 400 turns of 1 mm square wire. Two Kepco bipolar current supplies (36 V-12 A) connected in parallel supply currents as large as 18 A to the coil, generating fields up to ~1200 Oe. An electrolytic capacitor is connected in parallel to the coils to reduce the field ramp rate. A slow ramp rate prevents cantilever oscillations.

B. Salient aspects of the data

We now examine some typical data, to appreciate the salient aspects of the response of these materials. Response will be used to refer to the observed contraction or elongation of the magnetoelastomer in a magnetic field. Response is generally a combination of effects, but when the response is essentially due only to magnetostriction, or when the magnetostrictive contribution to the response is extracted from the raw data, we will refer to this as magnetostriction.

C. Saturation

We start with a magnetoelastomer of Fe particles chained in a uniaxial magnetic field, with the chains parallel to the long axis of the sample. At low fields the magnetostriction is observed to be proportional to the energy density of the field, as expected, Fig. 2. But at high fields the magnetostriction reaches a limiting value as the Fe saturates, Fig. 3(a). This high field data can be fit by the simple expression

$$\gamma = \frac{\alpha W}{1 + W/W_{ch}}, \tag{4}$$

where $W=BH$ is twice the field energy density and W_{ch} is the

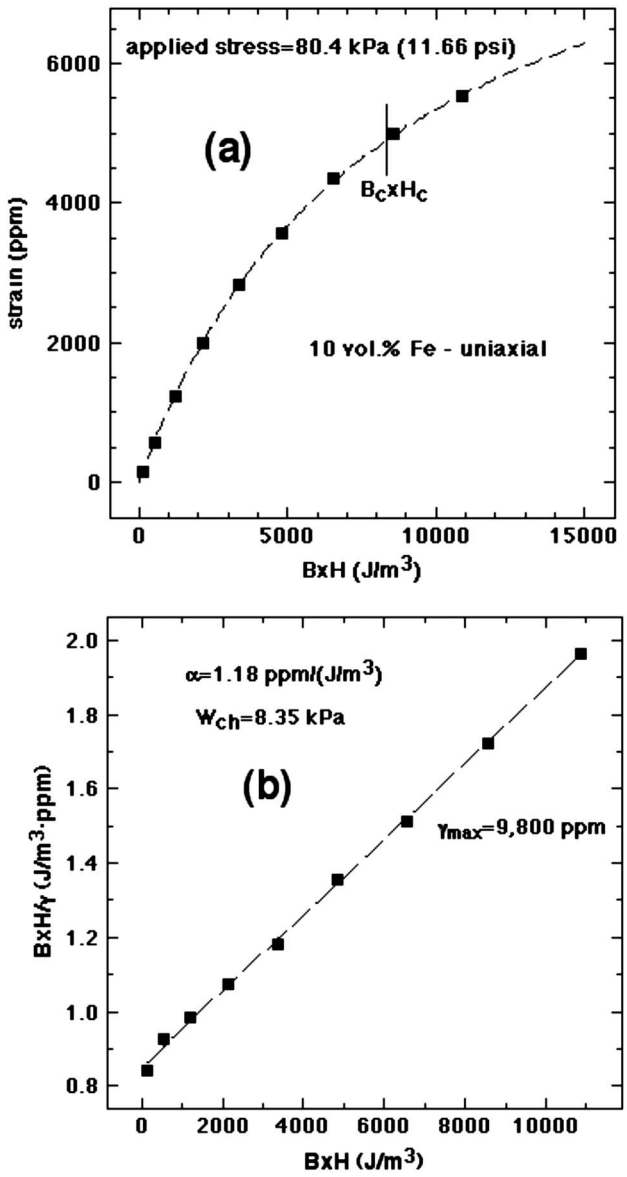

FIG. 3. (a) Response data for a 10 vol. % Fe composite shows the effect of magnetic saturation. The characteristic field product where the response is half of its maximum is indicated. (b) A linear plot on these axes indicates that Eq. (4) is an accurate description of the data and allows the fit parameters to be obtained from the slope and intercept. These parameters enable a saturation strain of 9800 ppm to be deduced.

characteristic value of this, at which the sample strain is 1/2 the maximum attainable. For composites having large susceptibilities one would expect α to be relatively large. At constant susceptibility W_{ch} will increase with the saturation magnetization of the particles.

If this relation is an accurate description of the data, then a plot of W/γ vs W should give a straight line. Data for a 10 vol. % uniaxial sample show that this is indeed the case, Fig. 3(b), giving $\alpha=1.18$ ppm/Pa and $W_{ch}=8.35$ kPa. In a saturating field the strain will approach $\gamma_{max}=\alpha W_{ch}$, which in this case is 9,800 ppm. This strain is five times greater than that obtained for terfenol-D.

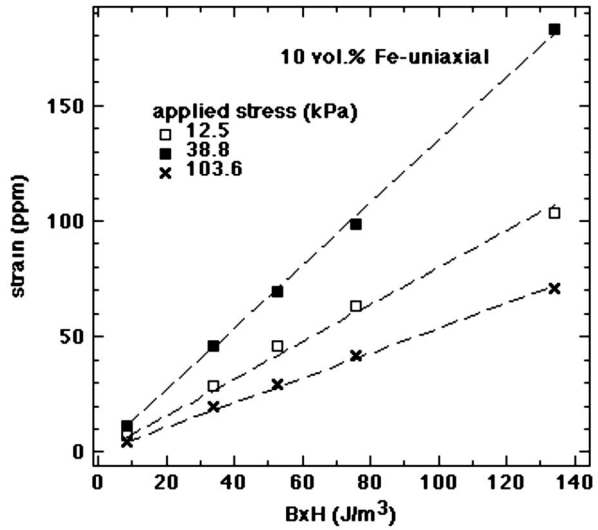

FIG. 4. Measurements of the response of a uniaxial Fe composite show a dependence on prestress. The response increases linearly with prestress for stresses below a yield stress. Note in particular the especially low response at the highest applied stress.

D. Prestress dependence

For a chain of hard spheres to contract there must be gaps between the particles, so it is not surprising that there should be some dependence of magnetostriction on sample prestress or prestrain. The low field data in Fig. 4 were taken at three widely different prestresses, and show a nonmonotonic dependence of the observed strain on prestress. In this case the elastic modulus of the sample is 1.7 MPa, so the sample prestrain varied from 7400 ppm to 61 000 ppm. This prestrain is thus much greater than that needed to create gaps large enough to accommodate the observed responses, which are less than 200 ppm. This dependence of the observed strain on sample prestress is a complicated aspect of these materials that we will discuss below.

E. Particles

The linear theory of magnetostriction shows that the stress depends on the particle susceptibility. The susceptibility of field-structured composites of Ni and Fe powders are very similar [6,7], yet our experiments show that Fe composites have six times greater magnetostriction than Ni composites (data for 20 vol. % composites). We believe that this unexpected difference is due to poor adhesion of the polymer to the Ni particles, which causes field-induced clumping transitions in the strained Ni composites.

F. Sample shape

The observed response can also depend on the sample shape. In Fig. 5 measurements on a sample with an aspect ratio of 14.3 are compared to those on a sample of aspect ratio 5.9. The high aspect ratio sample has significantly greater response, due to the reduced opposing effect of demagnetization fields. Accounting for demagnetization field effects is thus an important aspect of extracting magnetostriction from the response data.

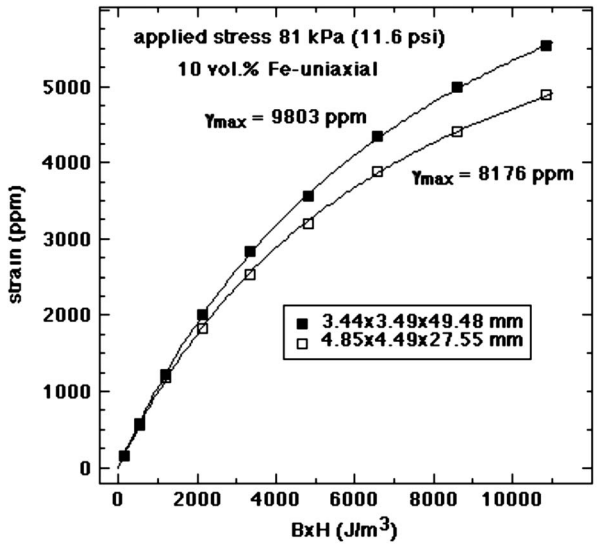

FIG. 5. Measurements on samples of aspect ratios 14.3 and 5.9 show how the sample shape can influence the response. The higher aspect ratio sample has a greater response at all fields, as expected from consideration of the opposing effect of demagnetization fields.

G. Composite structure

The structure of the particle agglomerates within the composite have an enormous influence on the response, Fig. 6. An unstructured sample has much smaller magnetostriction than a sample structured by a uniaxial field, and a sample structured by a biaxial field normal to the long axis of the sample even exhibits a negative response. Some samples ex-

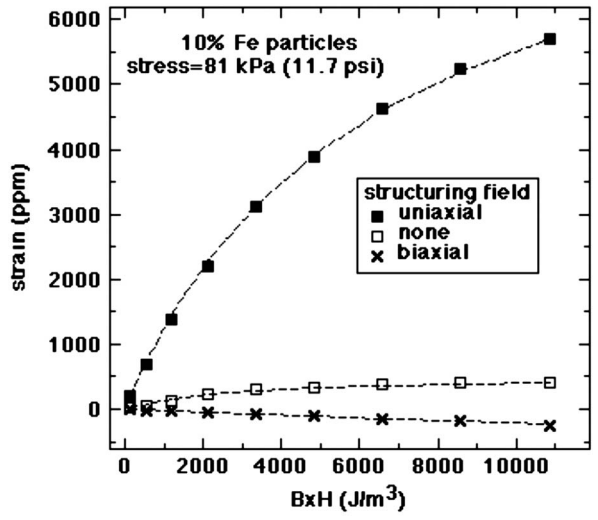

FIG. 6. The structure of the particle agglomerates has an enormous impact on the response. The composite made in a uniaxial field has a considerably greater response than the unstructured, random composite. The composite made in a biaxial field actually exhibits a negative response.

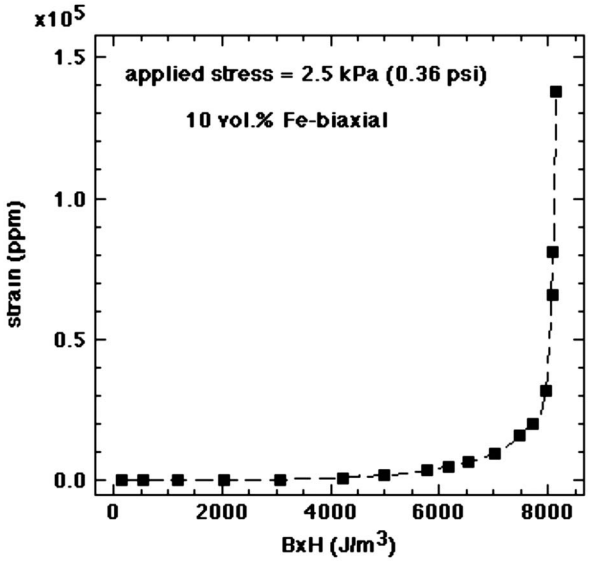

FIG. 7. Biaxial composites made at small particle loadings exhibit an anomalously large response at very small applied stresses and high fields.

hibit even more complex behavior, with an observed positive response at low fields and a negative response at high fields. But whether or not this mixed behavior occurs is also dependent on the prestress.

H. Extraordinary response

A few samples were found to exhibit an extraordinary response, Fig. 7. This extraordinary response occurs at lower particle loadings, low applied stresses, and high fields. It also only occurs for samples structured by a biaxial field.

It is clear that there are quite a few effects for which an explanation is needed. We will start by considering demagnetization field stresses, as an understanding of these is essential to the interpretation of all the response data.

V. DEMAGNETIZING FIELD STRESSES

We now consider the demagnetizing field stress on a prolate spheroid subjected to an initially uniform magnetic field. Our samples are solid rectangles, so this stress computation will not exactly correspond to experiment, but is nonetheless a good approximation.

The tensile stress on a prolate spheroid due to its demagnetizing field arises because an elongation of the sample will decrease its demagnetizing field, thus increasing its internal field and magnetic moment. The field inside a prolate spheroid is uniform when placed in an initially uniform field, which makes possible an analytical solution to internal field. This internal field can also be expressed in terms of a demagnetization factor that is *independent* of the material susceptibility [9]. The field inside a solid rectangular object is not uniform, and does not admit to an analytical solution. A demagnetization factor can be defined for the average internal field, but then this depends in a complex way on the material susceptibility [6].

We start by developing an expression for the internal field. For a prolate spheroid of aspect ratio $g>1$ with its long axis aligned with the field (which we take to be along the z axis) the demagnetization factor n is [9]

$$n = \frac{1}{g^2-1}\left[\frac{g}{2\sqrt{g^2-1}}\ln\left(\frac{g+\sqrt{g^2-1}}{g-\sqrt{g^2-1}}\right)-1\right]$$
$$\cong [\ln(2g)-1]/g^2 \quad \text{for } g \gg 1. \tag{5}$$

The macroscopic internal field is then given by the standard expression $\mathbf{H}_{\text{int}}=\mathbf{H}_0-n\mathbf{M}=\mathbf{H}_0-n\chi\mathbf{H}_{\text{int}}$, where χ is the composite susceptibility. If the applied field is low enough that the composite is far from saturation, then we can assume the composite susceptibility χ is independent of field, and

$$\mathbf{H}_{\text{int}} = \mathbf{H}_0/(1+n\chi). \tag{6}$$

To compute the stress we consider the energy change during strain. The energy of a linear magnetic material of moment $\mathbf{m}$ in an applied field $\mathbf{H}_0$ is $U=-\frac{1}{2}\mu_0\mathbf{m}\cdot\mathbf{H}_0$. This expression includes the work done by a perfect power supply used to keep the applied magnetic field constant. The applied field will thus cause a force $\mathbf{F}=-\frac{\partial U}{\partial Z}\hat{\mathbf{z}}$, where Z is the spheroid major diameter. A positive force indicates an elongational stress. In terms of the sample moment $\mathbf{m}=V\mathbf{M}$, the force is $F=+\frac{1}{2}\mu_0 H_0 V\frac{\partial M}{\partial Z}\hat{\mathbf{z}}$, where $V=\frac{\pi}{6}\rho^2 Z$ is the sample volume, ρ is the spheroid minor diameter, and the magnetization is $\mathbf{M}=\chi_c\mathbf{H}_{\text{int}}$. Using Eq. (6) for the internal field gives the force

$$\mathbf{F} = \frac{1}{2}\frac{\mu_0 H_0^2 V}{(1+n\chi)^2}\left[\frac{\partial\chi_c}{\partial Z}-\chi^2\frac{\partial n}{\partial Z}\right]. \tag{7}$$

Large aspect ratio samples. For incompressible samples having a large aspect ratio g it is simple to obtain an analytical result for the demagnetizing stress. In this limit the demagnetization factor is approximately $n_a=[\ln(2g)-1]/g^2$, and $\frac{\partial n_a}{\partial Z}=\frac{-3}{\rho g^3}(\ln 2g-3/2)$. Substituting this expression into Eq. (7) gives the measured stress

$$\sigma_{meas} = \frac{\sigma_{mag}}{(1+n\chi)^2}+\frac{\mu_0\chi^2 H_0^2}{(1+n\chi)^2}\frac{\ln 2g-3/2}{g^2}, \tag{8}$$

where the magnetostrictive stress is $\sigma_{mag}=\frac{1}{3}\mu_0 H_0^2\frac{\partial\chi}{\partial\gamma}$ and γ is the strain. This expression can be used to correct experimental data taken at low applied fields for the demagnetizing field strain, with the result

$$\gamma_{mag} = \left\{\gamma_{meas}-\frac{\mu_0 M^2}{E}[n-1/2g^2]\right\}\left(\frac{H_0}{H_0-nM}\right)^2, \tag{9}$$

where $\mathbf{M}=\chi\mathbf{H}_{\text{int}}$ and E is the tensile modulus.

A. Saturation

At magnetic fields large enough that the linear susceptibility approximation fails, the calculation of the stress becomes more complex. If we define the nonlinear susceptibility $\chi(H_{\text{int}})=M/H_{\text{int}}$, the internal field can be written as $\mathbf{H}_{\text{int}}=\mathbf{H}_0/[1+n\chi(H_{\text{int}})]$. For particle composites the susceptibility is small, typically less than 5, and for long prolate ellipsoids the demagnetization factor is small as well, so the product $n\chi$

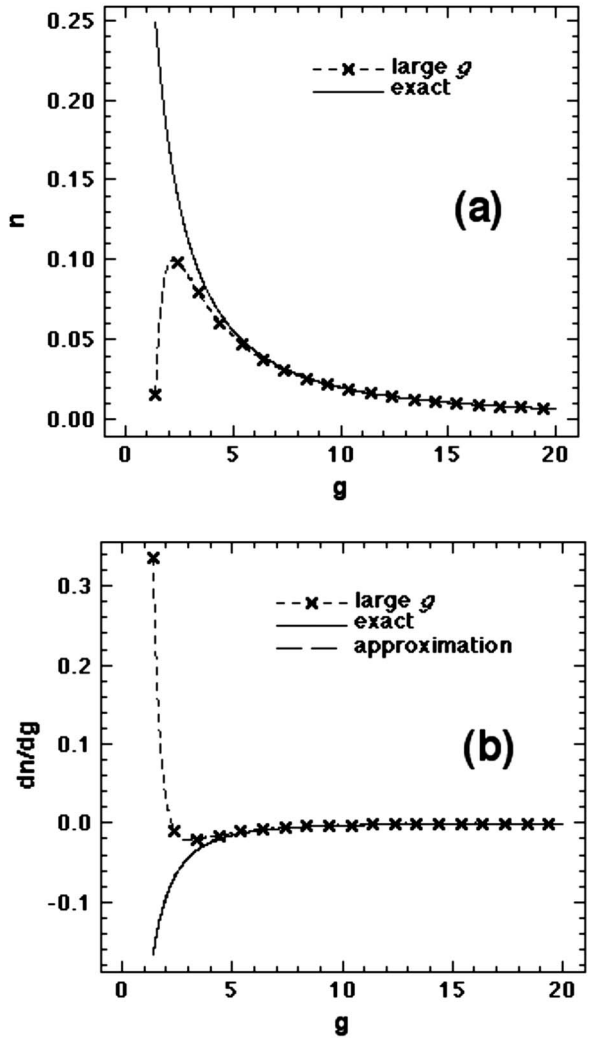

FIG. 8. (a) A comparison between the approximate (labeled "large g") and exact forms of the demagnetization factor in Eq. (5) show that the approximate form becomes very inaccurate at low aspect ratios. (b) The derivatives of the approximate and exact expressions in Eq. (5) differ substantially for aspect ratios less than 5. The closed-form expression in Eq. (10) (labeled "approximation") is sufficiently close to the exact derivative that the discrepancy cannot be seen on this plot.

is small. Thus with little error we can use the approximation $\mathbf{H}_{\text{int}}=\mathbf{H}_0/[1+n\chi(H_0)]$. For a change in the sample magnetization at constant applied field the force is still $F=+\frac{1}{2}\mu_0 H_0 V\frac{\partial M}{\partial Z}\hat{\mathbf{z}}$. Using these expressions we can show that Eq. (9) is approximately correct even for saturating fields.

B. Small aspect ratio samples

For samples with a small aspect ratio, say $g<4$, Eq. (9) is a really poor approximation, as Fig. 8(a) shows. On the other hand, differentiating the exact form, Eq. (5), of the demagnetizing factor n with respect to g would lead to a formidable expression. A good approximation to the exact derivative dn/dg, taken numerically, is all that is needed. Balancing accuracy against simplicity we came up with

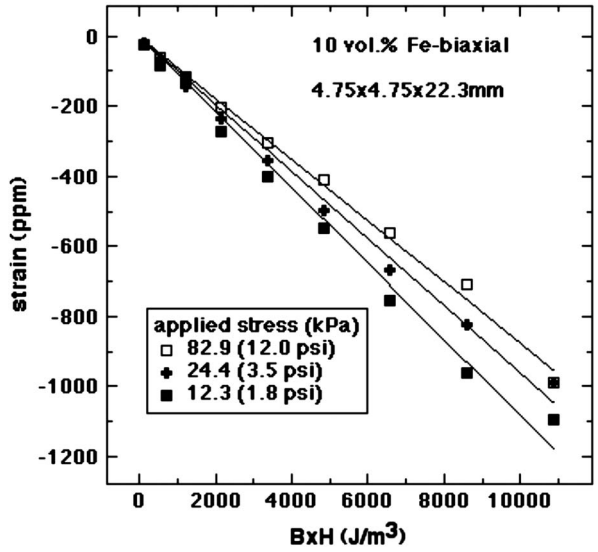

FIG. 9. Experiments performed on a low-aspect-ratio biaxial composite show a large negative response at all applied stresses, due to the minimal magnetostriction of this structure and the intentionally exagerrated effect of demagnetizing fields. From these data we conclude that the demagnetizing field strain is essentially independent of the applied stress.

$$\frac{dn}{dg}\approx-\frac{2n}{g}+\frac{1}{g^3}\left[1-\frac{7}{8}\ln(1+g^2)/g^2\right]. \tag{10}$$

This expression becomes exact for large g and is never off by more than $\sim$1.4%, as shown in Fig. 8(b). The formula for the effect of demagnetizing fields on the measured strain is

$$\gamma_{mag}=\left\{\gamma_{meas}-\frac{\mu_0 M^2}{E}\left[n-\frac{1}{2g^2}\left[1-\frac{7}{8}\ln(1+g^2)/g^2\right]\right]\right\}\times\left(\frac{H_0}{H_0-nM}\right)^2. \tag{11}$$

This expression is much more accurate than Eq. (9) for low aspect ratio samples.

A key prediction of Eq. (11) is that the demagnetizing field strain (or stress) is independent of the sample prestress. Experimental data in support of this are shown in Fig. 9 for a 10 vol. % biaxial composite with an aspect ratio of 4.7. Here the observed response is entirely negative (elongation), being dominated by demagnetization fields. Because magnetostriction does depend on the sample prestress, the combination of the two effects can lead to complicated trends, as shown below.

C. An example

A biaxial, 30 vol. % Fe particle composite is an ideal example of the importance of demagnetization field corrections, since it should exhibit small magnetostriction and thus the demagnetization fields should produce a significant contribution to the response. The data for this sample, Fig. 10(a), show a complex behavior with both negative and positive responses obtained at some sample preloads. The modulus

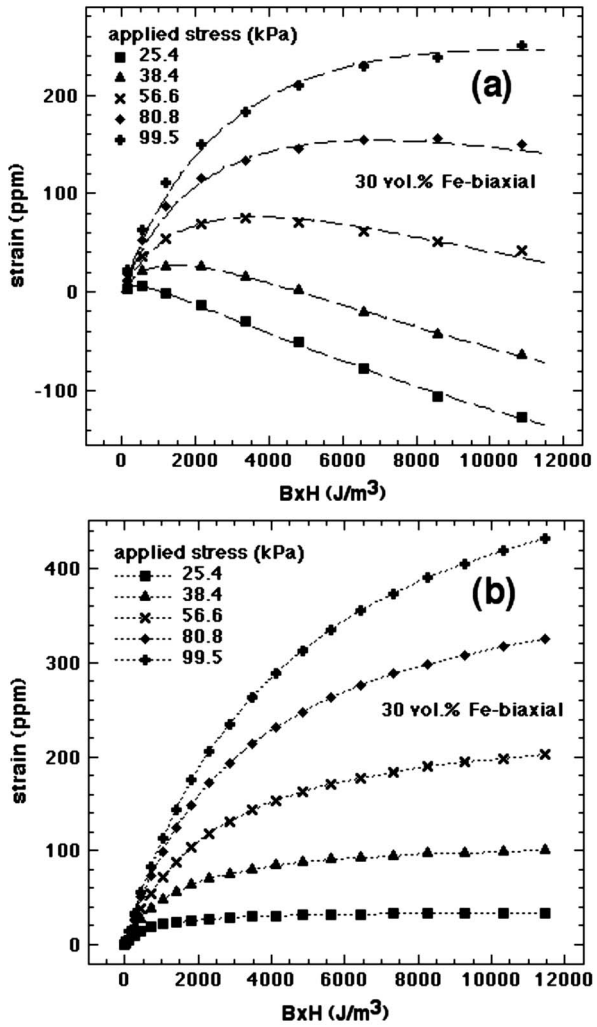

FIG. 10. (a) For a 30 vol. % biaxial field-structured composite the response data depend non-monotonically on the field, with both negative and positive responses at some applied stresses. (b) The magnetostriction effect extracted from the response data by removing the influence of demagnetizing fields is positive and monotonic.

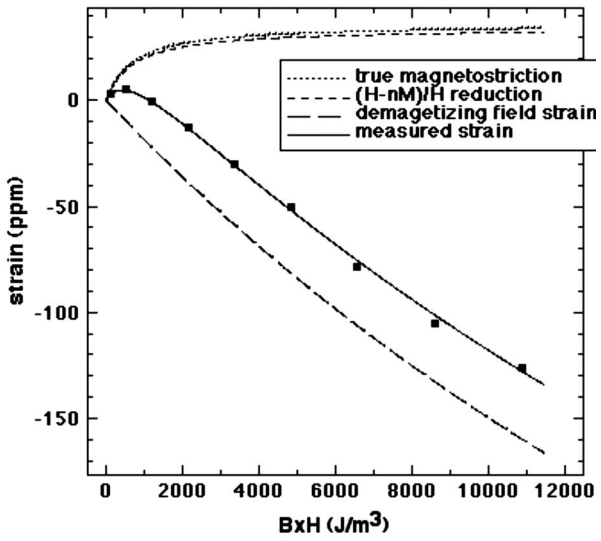

FIG. 11. The various contributions to the response curve in Fig. 10(a) that was taken at an applied stress of 25.4 kPa are shown. The demagnetizing field strain dominates magnetostriction, which reaches a maximum of only 27 ppm. The correction (H-nM)/H for the field penetration is negligible. This demagnetizing field strain was subtracted from all of the response data in Fig. 10(a) to generate the magnetostriction data in Fig. 10(b).

for this composite is 7.5 MPa, so the range of sample prestrains is from 3400–13 300 ppm.

To correct this response data for demagnetizing field effects requires an expression for the sample magnetization. In an earlier paper [11] we studied the magnetization behavior of field-structured particle composites and found that the expression

$$M = \frac{\chi H}{\sqrt{1 + (\chi H/\phi M_{sat})^2}} \tag{12}$$

is accurate. Here ϕ is the volume fraction of particles, χ is the composite susceptibility, and M_{sat} is the saturation magnetization of the particle material. M_{sat} for Fe is 1.72×10^6 A/m and the measured composite susceptibility along the applied field χ is 3.03 for this 30 vol. % biaxial composite.

We first examine the largely negative response at the lowest prestress, Fig. 10(a), since this is mostly due to demagnetization fields. This curve is fit to the sum of two functions: Eq. (4), whose two parameters we seek, and Eq. (11), whose parameters are known. Some adjustment to the sample aspect ratio is required, as the samples are solid rectangles, not prolate spheroids. The result of this analysis, Fig. 11, shows that demagnetization fields dominate the response of this sample. The extracted magnetostriction curve is positive and monotonically increasing, with a maximum strain of only 27 ppm at this prestress. Fits to the remaining response curves in Fig. 10(a) were made with exactly the same demagnetization strains, with the extracted magnetostriction curves shown in Fig. 10(b). The magnetostriction of this sample is really quite poor, as expected from theory [8].

Finally, it is of interest to examine the dependence of the demagnetization strain on particle loading for the aspect ratios of our standard samples. These computed curves are shown in Fig. 12 for both random and uniaxial composites, using the measured tensile moduli and composite susceptibilities. For the uniaxial samples the demagnetization field correction becomes significant only at 30 vol. %.

VI. EXTRAORDINARY RESPONSE

Some of the samples we synthesized to test our understanding of magnetostriction in field-structured composites exhibited an extraordinary positive response at low preloads and high fields. This surprised us because this effect only occurred for samples we expected to have minimal magnetostriction. This extraordinary response only occurs when the transverse susceptibility (i.e., normal to the long axis) of the magnetoelastomer significantly exceeds the longitudinal susceptibility.

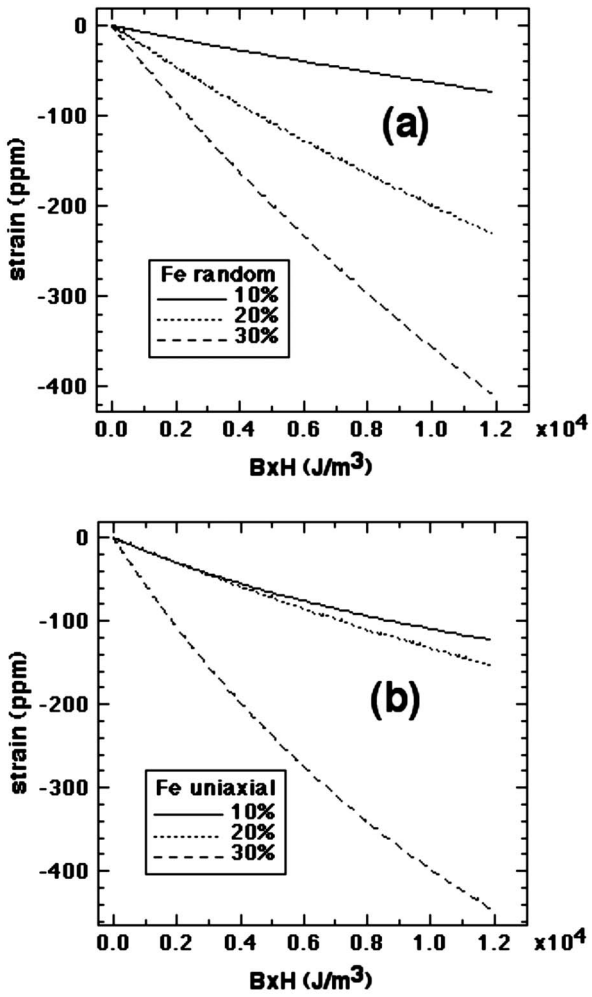

FIG. 12. Modeling the demagnetization field strain for (a) random and (b) uniaxial composites shows that the strain becomes increasingly significant as the particle loading increases. There is also a dependence on structure, since this affects the sample magnetization.

A. Susceptibility anisotropy

For most samples the field exerts a stabilizing torque, since a magnetic material will tend to align along its long axis. The cause of the extraordinary response is a destabilizing torque that is due to an inverse susceptibility anisotropy in some samples.

The parallel and perpendicular sample susceptibilities $\chi_{\parallel}$, $\chi_{\perp}$ are functions of composition and shape. Taking both of these factors into account gives

$$\chi_{\parallel} = \frac{\chi_{c,\parallel}}{1 + n_{\parallel}\chi_{c,\parallel}}, \quad \chi_{\perp} = \frac{\chi_{c,\perp}}{1 + n_{\perp}\chi_{c,\perp}}, \tag{13}$$

in terms of the susceptibilities intrinsic to the composite itself, $\chi_{c,\parallel}$ and $\chi_{c,\perp}$. In the absence of an applied stress the sample will align along the axis of greatest susceptibility. The magnetic field is applied along the longitudinal axis, but if the perpendicular susceptibility is larger, i.e., $\chi_{\perp} > \chi_{\parallel}$, the field will exert a destabilizing torque on the sample.

The question arises as to whether it is possible for this destabilizing torque to arise in a long thin FSC. For a long, thin cylinder the demagnetization factors are very close to $n_{\parallel}=0$, $n_{\perp}=1/2$. For a 10 vol. % biaxially structured composite of particle sheets we have found [11] that the susceptibility normal to the sheets is 0.335 (MKS), whereas in the plane of the sheets it is 1.593. If the sheets are formed normal to the cylindrical axis, the sample susceptibility is $\chi_{\perp} = 1.593/(1+0.5\times 1.593) = 0.8875$ which is much greater than the longitudinal susceptibility of 0.335. Such a sample will exhibit a destabilizing torque in an applied field if the applied stress is small enough.

At higher particle concentrations a destabilizing torque should not occur. For example, for a 20 vol. % composite the susceptibility normal to the sheets is 1.380 (MKS) and in the plane of the sheets it is 2.750. If the sheets are again formed normal to the cylindrical axis, the sample susceptibility is $\chi_{\perp} = 2.750/(1+0.5\times 2.750) = 1.158$ which is now lower than the longitudinal susceptibility of 1.380, so the torque will be stabilizing, even at zero applied stress.

B. Torque balance

The magnetic torque on the sample can be computed by considering the magnetostatic energy of a sample inclined at an angle θ to the applied field. The magnetostatic energy is $U = -\frac{1}{2}\mu_0 \mathbf{m}\cdot\mathbf{H}_0$ where $\mathbf{m}$ is the sample moment. Let our Cartesian coordinates (x,y) be such that the applied field is in the y direction. The coordinates (x',y'), are defined such that the sample is along the y' direction. The sample moment is then $\mathbf{m} = vH_0(\chi_{\parallel}\cos\theta\hat{\mathbf{y}}' - \chi_{\perp}\sin\theta\hat{\mathbf{x}}')$, where v is the sample volume. The energy is thus $U = -\frac{1}{2}vH_0^2(\chi_{\parallel}\cos^2\theta + \chi_{\perp}\sin^2\theta)$ and the magnetic torque is

$$\tau_m = \mu_0 v H_0^2 \cos\theta \sin\theta(\chi_{\perp} - \chi_{\parallel}). \tag{14}$$

As expected, a positive, destabilizing torque occurs when the transverse susceptibility exceeds the longitudinal. The stress applied to the sample exerts the negative torque $\tau_s = -Fl\sin\theta$, where l is the sample length. Balancing the mechanical and magnetic torques gives the equilibrium angle

$$\cos\theta = \frac{\sigma}{\mu_0 H_0^2(\chi_{\perp} - \chi_{\parallel})} \tag{15}$$

in terms of the sample stress σ. When this expression gives a positive value of $\cos\theta$ that is less than unity, an instability will occur. This condition occurs with large fields and small applied stresses. The sample strain is just $1-\cos\theta$.

For the 10 vol. % sample of sheets, $\chi_{\perp} - \chi_{\parallel} = 0.553$. At an applied stress of 3.45 kPa (0.5 psi) the critical field will be 70.5 kA/m (883 Oe). Larger fields will show a clear instability, as the data in Fig. 7 demonstrate.

VII. RESULTS

In this section we discuss the magnetostriction results we have obtained for a variety of composite structures, with volume fractions ranging from 10–45%. In these controlled stress experiments the strain is directly measured, but in ad-

dition there are a number of computed quantities that are of interest. These include the maximum strain at saturation, the characteristic field product BH (twice the field energy density), the magnetic field contribution to the stress and modulus, the work performed, and the energy efficiency.

Before giving these factors it is interesting to note that the self-consistent point dipole model actually overestimates magnetostriction. Consider the 10 vol. % composite structured by a uniaxial field, for which the predicted stress is $6.9 \times \frac{1}{2}\mu_{eff}\mu_0 H_0^2$. Experiments show that the effective relative permeability for this composite is $\mu_{eff}=2.36$ and the tensile modulus is 1.7 MPa (245 psi). Using these parameters we predict a strain of $\gamma(\text{ppm})=(4.8\ \text{m}^3/\text{J})B\times H$, where B is the magnetic induction field created by the magnet in the absence of the sample. Experimental data at low fields and optimal sample preload give $\gamma(\text{ppm})=(1.2\ \text{m}^3/\text{J})B\times H$, so the real material falls well short of expectations. We believe the discrepancy is related to the fact that the observed magnetostriction is dependent on prestress, and the reasons for this are complex, as discussed briefly below.

A. Saturation strain and characteristic field product

The maximum strain at magnetic saturation and the characteristic field product are obtained from fitting to Eq. (4), as described above. For the 10 vol. % chain sample the result is in Fig. 13(a). Here it is seen that the greatest saturation strain occurs at an applied stress of ~80 kPa, corresponding to an applied tensile strain of 4.7%. At this prestress the characteristic field product $B\times H$ is 6.4 kPa, so the composite reaches half its saturation strain at a field of ~72 kA/m (900 Oe). A field of this magnitude is easily achieved with an open-air Helmholtz coil, making these materials a practical choice for actuator applications.

B. Magnetic modulus and stress

Because measurements at low applied stresses show a linear dependence of the sample strain on the applied stress, invoking a field-dependent magnetic tensile modulus E_m is a useful way to describe the data. For a sample under constant stress, the effect of the magnetic field is to change the strain alone. This strain change is $\Delta\gamma=\sigma[1/E_0-1/(E_0+E_m)]$, so the magnetic modulus is

$$E_m=\frac{\Delta\gamma E_0^2}{\sigma-\Delta\gamma E_0}, \tag{16}$$

where E_0 is the tensile modulus in the absence of an applied field. The magnetic modulus for the 10 vol. % Fe chain composite at saturation is given in Fig. 13(b), using the measured tensile modulus of 1.7 MPa (245 psi). E_m increases with magnetic field and can be as large as 0.4 MPa at modest fields. Figure 13(b) shows a pronounced yield behavior, and the yield stress is found to increase with magnetic field, so it would be careless to use the magnetic modulus to compute stresses and strain without taking this yield behavior into account.

When the magnetic field is turned on, the sample contracts, so part of the stress initially supported by the elastomer is taken up by the magnetic interactions between the particles. This magnetic stress load is

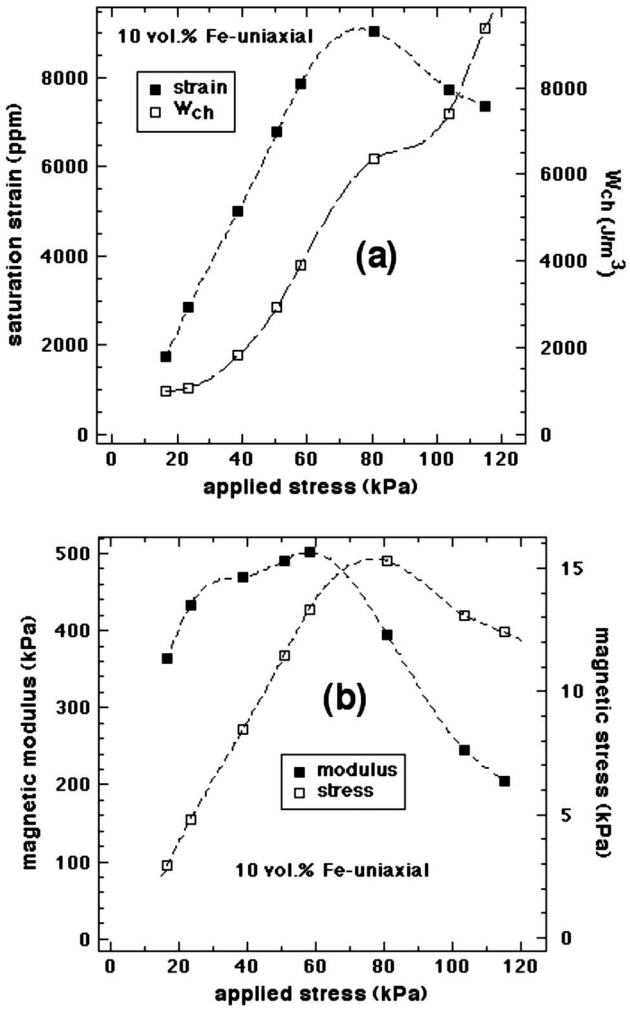

FIG. 13. (a) The saturation strain of a 10 vol. % Fe composite approaches a maximum of 10 000 ppm. The characteristic field products, Eq. (4), where this composite reaches half maximum response, increase with the load, but remain well within the range of open air Helmholtz coils. (b) The magnetic modulus of this composite reaches a maximum of 500 kPa at a load of 60 kPa, but the magnetic stress maximizes at only 15 kPa, due to the small saturation strain.

$$\sigma_m=\sigma E_m/(E_0+E_m)=\Delta\gamma E_0, \tag{17}$$

a formula which is intuitive, since a force added to a harmonic well merely generates a displaced harmonic well with the same stiffness. The data in Fig. 13(b) show that a maximum magnetic stress of 15 kPa can be obtained at a particle loading of 10 vol. %.

It is interesting to look at the work done per unit volume of sample during this strain. This "work density" is the product of the strain and the applied stress. For the 10 vol. % Fe sample the work density is $u=9800\ \text{ppm}\times 80.4\ \text{kPa}=0.8\ \text{kPa}$ at magnetic saturation.

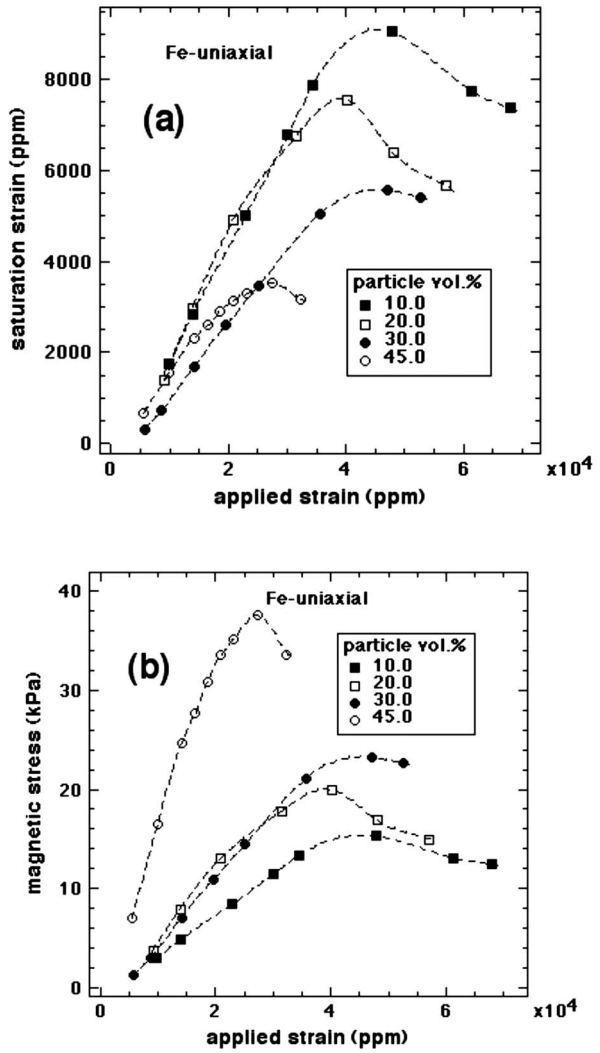

FIG. 14. (a) The saturation strain as a function of the applied strain for uniaxial composites. The saturation strain decreases significantly with increasing particle loading and maximizes at lower applied strains. (b) The magnetic stress increases with particle loading and exhibits well-defined maxima. This maximum is at considerably lower applied strains for the 45 vol. % composite.

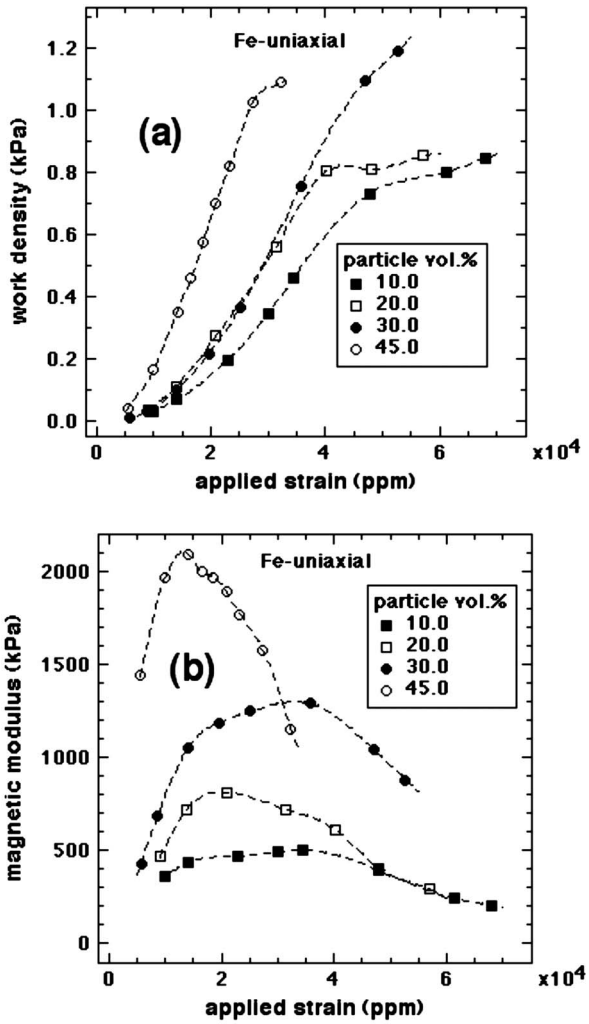

FIG. 15. The work density (a) and magnetic modulus (b) as a function of applied strain for uniaxial composites of a range of particle loadings. These data show that performance increases with particle loading, even though the magnetostrictive strain decreases with particle loading. The magnetic modulus of the 45 vol. % sample is especially high, but reaches a maximum at a low strain, so the work density is high at might be expected.

C. Effect of particle loading

It would be expected that the magnetic response of these composites increases in proportion to the particle loading, but in reality the performance increases are mixed. As the particle loading increases, the sample response actually decreases, Fig. 14(a), but the magnetic stress increases, Fig. 14(b), because of the increase in the composite tensile modulus. Increasing the particle concentration thus yields an actuator that can handle larger loads, but with smaller displacements. In fact, the work density also increases with particle loading, Fig. 15(a), reaching a value of over 1 kPa at an applied strain of ~2% for a particle loading of 45 vol. %. The magnetic modulus, Fig. 15(b), increases sharply with concentration, peaking at over 2 MPa (290 psi) at 45 vol. %, compared to the zero field tensile modulus of 10.8 MPa.

D. Role of composite structure

Composite structure is of cardinal importance in the response of magnetoelastomers to magnetic fields. To illustrate this we compare the magnetostriction of unstructured (~random) composites to field-structured composites.

In Fig. 16 the raw response (a) and extracted magnetostriction (b) curves are shown for an unstructured 10 vol. % Fe composite. (The magnetostriction was extracted from the response curves in the manner described above.) The magnetostriction of this unstructured composite is ~5 times smaller than that of the 10 vol. % uniaxial composite, Fig. 5. We are unable to provide data for a biaxial sample at this particle loading because of the torque instability exhibited by this sample. However, we would expect that the biaxial composite would have very low magnetostriction.

At 30 vol. % the torque instability does not exist, so it is possible to collect response data for a biaxial sample. These

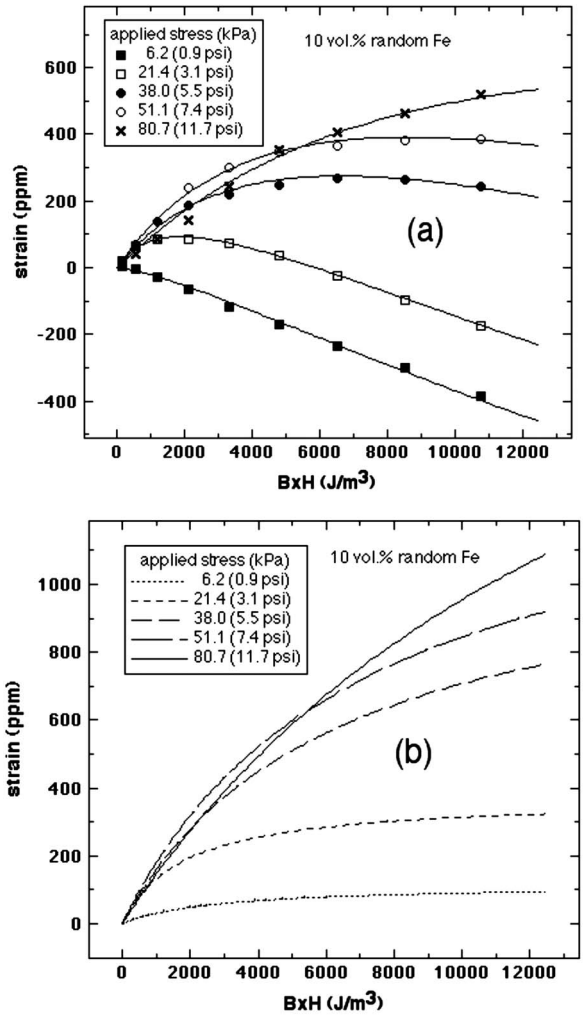

FIG. 16. Response (a) and extracted magnetostriction (b) for an unstructured 10 vol. % Fe composite. The magnetostriction of this unstructured composite is roughly 1/6 that of a uniaxial composite at the same particle loading.

measurements show that at the same applied stress the magnetostriction of a biaxial sample is roughly 6.6 times smaller than a uniaxial sample. The tensile modulus of the biaxial composite, 7.5 MPa, is larger than that of the uniaxial composite, 4.2 MPa, so the measured magnetic stress ratio [see Eq. (17)] of the uniaxial to the biaxial composite is $6.6 \times 4.2/7.5 = 3.7$. The theoretical magnetic stress ratio, based on simulated 30 vol. % structures, is 4.4, which is in reasonable agreement with experiment. In the linear response regime the biaxial composite strain response is $\gamma(\text{ppm}) = (0.13\ \text{m}^3/\text{J})B \times H$ whereas the uniaxial obeys $\gamma(\text{ppm}) = (0.66\ \text{m}^3/\text{J})B \times H$, both at an applied stress of 100 kPa. Accounting for the modulus difference gives a magnetic stress ratio of 3, somewhat smaller than at larger fields.

E. Triaxial composites

As mentioned above, we have been successful in using triaxial magnetic fields to enhance the susceptibility of particle composites to levels exceeding those obtained in uniaxial fields [7]. According to the trends of the self-consistent point dipole theory given above, triaxial composites should thus have greater magnetostriction than uniaxial composites. To test this hypothesis we synthesized composites under two triaxial field conditions: balanced 2D heterodyning, and 3D heterodyning with a +25% field bias along the long axis of the sample. Because the uniform field region of our triaxial magnet is small, we had to reduce the size of our samples to $3.3 \times 3.3 \times 24$ mm, which lowered their aspect ratio. To facilitate direct comparison, we also synthesized a uniaxial composite of the same dimensions.

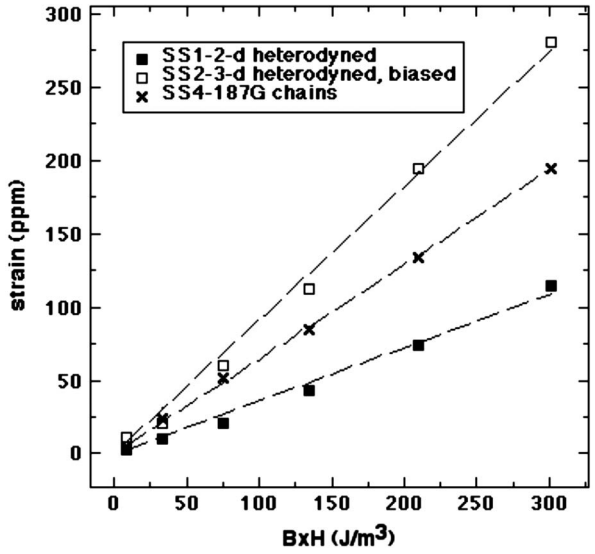

FIG. 17. The magnetostriction at low fields is compared for composites structured by three types of magnetic fields: a uniaxial, 2D heterodyned, and 3D heterodyned with a bias (field enhancement) along the long axis of the composite. Biased heterodyning leads to composites with greater magnetostriction than those synthesized in a simple uniaxial field. This result is expected, since this type of structuring field maximizes the composite susceptibility.

The measured specific susceptibilities of these three composites are 15.8 for the 2D heterodyned, 17.2 for the uniaxial, and 23.1 for the 3D heterodyned with +25% field bias. We expect that the magnetostriction data will reflect this trend, and it does, Fig. 17. The balanced triaxial field with 2D heterodyning has reduced magnetostriction relative to the uniaxial sample, and the biased 3D heterodyned composite has increased magnetostriction. We cannot make a detailed comparison to theory, as our mean-field approach is problematic for composites made in triaxial fields [7].

VIII. DISCUSSION

A remaining issue is why the observed strain depends on the sample preload, when the preloads are clearly sufficient to accommodate a much greater contraction without the particles contacting. This is a complex effect that we believe has to do with field-induced particle clumping transitions. The possibility of clumping was mentioned in our paper on striction, but here we would like to start to develop that idea quantitatively, focusing only on a single chain.

There are two forces on an enchained particle subjected to a longitudinal magnetic field: a destabilizing attractive dipolar interaction with the other particles in the chain, which tends to bring vicinal particles into contact, and a stabilizing elastic interaction with the gel, which tends to localize a particle at the mid-point between the two vicinal particles. Each of these potentials has a curvature, and when the sum of these curvatures is zero the force on a particle is zero and the chain become unstable to fluctuations, a so-called "soft mode."

A. Constrained chain

In the interest of simplicity we will first consider a simpler instability: that of a single "focus" particle in an elongated chain with all of the other particles held fixed. As an initial condition all of the particles are initially equally spaced. We seek the force on the focus particle displaced a distance ε from the midpoint between its nearest neighbors. If the displacement is positive and the force is negative, then the midpoint is a stable position, and vice versa. This chain is taken to be aligned along the z axis, and is subjected to an applied field $\mathbf{H}_0 = H_0\hat{\mathbf{z}}$.

B. Magnetic force

The magnetic force on the focus particle is proportional to the gradient of the local field. The local field is the sum of the applied field plus the fields from all of the other dipoles. The "dimagnetophoretic" force on a particle is given by the well-known expression $\mathbf{F}_m = \mu_0 \mathbf{m} \cdot \nabla \mathbf{H}_{loc}$, which reduces to $\mathbf{F}_m = \mu_0 m(\partial H_{loc}/\partial z)\hat{\mathbf{z}}$, with $\mathbf{H}_{loc}$ the local field.

To compute the local field we must first determine the field produced by each dipole. Each dipole of induced moment $\mathbf{m} = m\hat{\mathbf{z}}$ will produce a field that along the chain axis is $\mathbf{H}_m = \frac{1}{2\pi r^3} m\hat{\mathbf{z}}$. A self-consistent point dipole calculation shows that the magnitude of the moment of each interior dipole is $m = v\chi_p H_0/[1 - \chi_p \zeta(3)/6\delta^3]$ where $v = \frac{\pi}{6}d^3$ is the particle volume, $\zeta(x)$ is the Reimann zeta function, and the chain *elongation* is $\delta = 1 + \gamma$ where γ is the chain strain (at $\delta = 1$ the particles just contact.) The particle susceptibility $\chi_p = 3\beta$ where β is the permeability contrast factor defined above. From symmetry the local field at a dipole site is an even function and can thus be expressed as a series of the square of the particle displacement. To first order in ε^2 the local field at the focus particle is

$$\mathbf{H}_{loc}(\varepsilon) = \frac{\mathbf{H}_0}{1 - \dfrac{\chi_p \zeta(3)}{6\delta^3}} \left[1 + \frac{\chi_p \zeta(5)}{\delta^5 d^2} \varepsilon^2 \right]. \tag{18}$$

By differentiating the local field the magnetic force on the particle is found to be

$$\mathbf{F}_m = +\zeta(5) \frac{\pi d}{3\delta^5} \left[\frac{\mu_0 \chi_p^2 H_0^2}{1 - \dfrac{\chi_p \zeta(3)}{6\delta^3}} \right]^2 \varepsilon \hat{\mathbf{z}}. \tag{19}$$

Note that this magnetic force is always destabilizing.

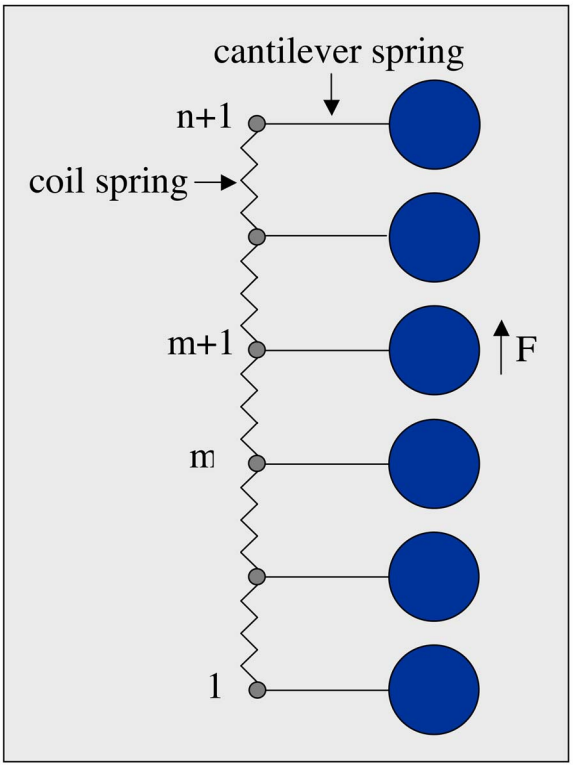

FIG. 18. (Color online) Illustration of the cantilever model showing both the cantilever springs and coil springs. In the cantilever model the coil springs are much stiffer than the cantilever springs, and are included only to facilitate an understanding of the stress calculation.

C. Elastic force

The elastic force on a single particle embedded in a gel and displaced a distance ε in the z direction is $\mathbf{F}_g = -3\pi d G \varepsilon \hat{\mathbf{z}}$, where G is the gel modulus. For a particle in a chain, G will have to be renormalized due to debonding of the gel from the particle in the particle gap region, so G may be regarded as an effective parameter. In this view of the gel each particle is localized as if by a cantilever spring. Elastic interactions between particles are not included, so we simply call this the cantilever model. An illustration of the cantilever model is given in Fig. 18.

D. Particle potential

Before giving a detailed analysis of the stability of an *athermal* enchained particle, it is helpful to outline the three possible regimes: stable, bistable, and unstable. Consider a chain that is strained to create equal gaps between the particles. If the field applied parallel to the chain is small, the potential will form a well with upward curvature, and the focus particle will be stable. At a critical magnetic field, the curvature of the potential at the edge of the well vanishes, Fig. 19, so that the focus particle would remain in contact with a neighboring particle, if displaced to that position. This critical field marks the declumping transition. At fields somewhat larger than this declumping field the potential is bistable, which can cause hysteresis in the particle position.

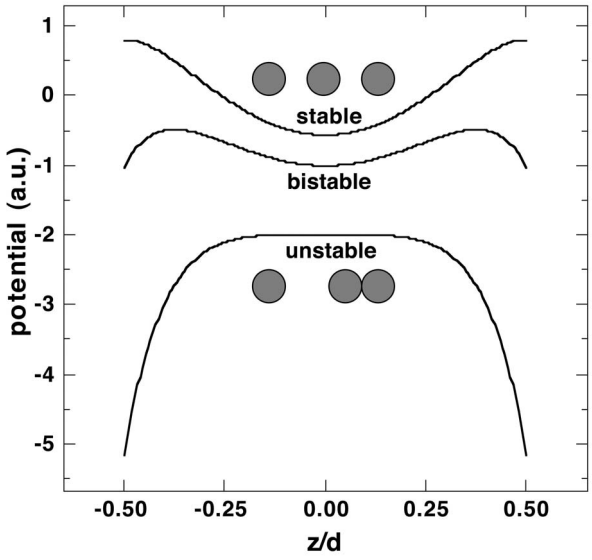

FIG. 19. The potential of an enchained particle is deformed by the application of a magnetic field. Three regimes are possible, and occur with increasing magnetic field: stable, bistable, and unstable. Chain elongation has an opposite, stabilizing effect.

Finally, a second critical field is reached where the potential has zero curvature at the middle. This field marks the clumping transition, where the particle becomes unstable at its midpoint and will move into contact with one of its neighbors. Thus if an increasing field is applied parallel to the chain, the focus particle will clump at a field that is much larger than the field at which it will declump as the field is reduced.

E. Clumping transition

The focus particle becomes unstable when the magnetic force dominates the gel force. The clumping field that marks this transition is thus

$$\mu_0\beta^2 H_{clump}^2 = \frac{G}{n}\frac{\delta^5}{\zeta(5)}[1-\beta\zeta(3)/2\delta^3]^2. \tag{20}$$

Note that this transition is strongly dependent on the chain prestrain, which tends to stabilize the particle by reducing the magnetic interactions.

We have introduced a factor n in Eq. (20). This factor is 1 for the single particle fluctuation with the rest of the particles constrained—the case at hand. But for the physically more realistic case of a chain of unconstrained particles, the clumping transition is given by Eq. (20) with $n=2$. In this case the clumping transition exhibits itself as a clustering of particles into dimers.

Particle dimer formation is just the first of a non-ending succession of clumping transitions, each with its own stability condition. At successively higher fields, the dimers will form tetramers, the tetramers will form octamers and so forth.

F. Declumping transition

As the field is ramped back down, there is a succession of declumping transitions. But each of these transitions occurs at a lower field than the corresponding clumping transition. A tedious calculation shows that the declumping transition for dimers is

$$\mu_0\beta^2 H_{declump}^2 = \frac{32}{31}\frac{G}{n}\frac{\delta^5}{\zeta(5)}\left\{1-\beta\zeta(3)/2\delta^3 \times\left[1+\frac{6}{\zeta(3)}\left(\frac{\delta-1}{\delta}\right)^2\right]\right\}^2. \tag{21}$$

Declumping occurs at a smaller field than clumping, and the chain is hysteretic, in the true sense that energy is dissipated.

G. Simulations

The implications of this cantilever model for magnetostriction are interesting. To explore this, a dynamics simulation was written that included, in addition to the magnetic and gel forces, both hard sphere interactions and viscous dissipation in the gel, the latter of which serves to damp the phonons that would otherwise arise from the clumping instabilities. This simulation is done in the self-consistent point dipole approximation, and the chain is strained by displacing the chain ends alone—the other particles are unconstrained. The gel is assumed to deform affinely with the strain, so that the positions of the harmonic wells defined by the cantilever springs move in proportion to the strain. The force acting on each particle is the sum of the gel force, the dipolar interactions with all of the other particles, the hard sphere interactions with the nearest neighbors, and the viscous drag from the gel viscoelasticity.

H. Stress calculation

Before giving simulation results we must discuss the problem of stress calculation for the cantilever model. In general, the stress in a chain of particles is computed across any particular plane by simply summing the force of interaction between each particle on one side of the plane with all of the other particles on the other side. The force of interaction between the two semichains is then normalized by the area associated with the single chain to generate a stress. This computational prescription seems simple enough, but in the cantilever model the force on a particle due to the gel is not a pairwise interaction with another particle. How then does this gel force contribute to the stress?

To compute the gel stress we must account for the fact that the gel itself provides the support for the cantilevers. To model this we imagine that the cantilevers are connected to the nodes of a chain of coil springs, as depicted in Fig. 18. Each of the n Hookean springs has a force constant K and thus in the unperturbed state the tension in each spring is Kl_0, where l_0 is the unperturbed spring length. Now suppose the particle attached to the cantilever that is attached to node $m+1$ is displaced by a force F applied along the chain direction. The effect of this cantilever force is to alter the tension in the coil springs above and below this node. The tension

change in each coil spring contributes to the magnetic stress in a plane that bisects that spring.

The computation of the change in the spring tension is straightforward. Let x and y denote the coil spring length below and above node $m+1$, respectively. The total chain length, which is fixed, is then $L=nl_0=mx+(n-m)y$. A force balance gives $F=K(x-y)$. Combining these two equations and solving then gives $y=l_0-\frac{m}{n}\frac{F}{K}$. The tension of the springs above node $m+1$ change by $-\frac{m}{n}F$ and below node $m+1$ they change by $+\frac{n-m}{n}F$. Two points are noteworthy. First, the tension change in each spring is independent of the initial (zero field) spring tension. Second, this tension change depends on the position of the particle to which the force is applied, which is an unusual aspect of the cantilever model. The gel contribution to the stress across a plane that intersects spring m, which connects nodes m and $m+1$, is

$$\sigma_{gel}=\sum_{j=1}^{m}-\frac{j-1}{n-1}F_j+\sum_{j=m+1}^{n}\frac{n-j}{n-1}F_j. \tag{22}$$

The remaining stress contributions are from the dipolar and hard sphere interactions between particles separated by the stress plane. The sum of these terms gives a sample magnetic stress that numerical computations show is independent of the location of the stress plane, which is an important check on Eq. (22).

I. Simulation results

Typical results of this simulation are shown in stress versus elongation data in Fig. 20. In this simulation a chain subjected to a constant field is continuously elongated from a state of zero strain to some maximum strain, and then the strain is reversed.

Upon extension a series of declumping transitions are observed, until at full elongation the chain consists of equally spaced particles. These transitions cause the abrupt changes in the stress. Clumping transitions occur at lower elongations upon contraction, as expected, causing true hysteresis in the stress curves (the contraction stress is lower, as it must be). Two points are important. First, because of the energy dissipation it is not possible to obtain the stress from a strain derivative of the dielectric constant. Second, the stress still decays monotonically with the strain, unlike the experimental data, so this single chain model does not explain the preload dependence of our measured magnetostriction. Current work is focused on understanding collections of interacting chains. These calculations show some promise of explaining the unexpected dependence of magnetostriction on preload.

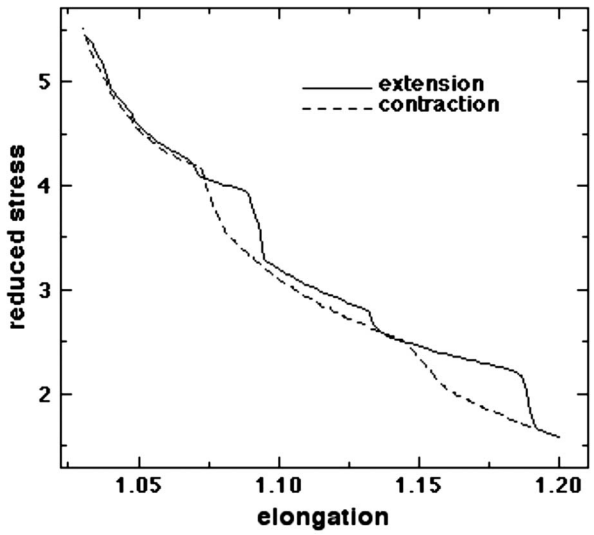

FIG. 20. Simulation of the cantilever model shows abrupt stress changes that are due to successive clumping transitions. Here the reduced stress, $\sigma/[(6\phi/\pi)\mu H^2]$, is plotted against the elongation. The hysteresis occurs because the fields at which the clumping and declumping transitions occur are somewhat different.

IX. CONCLUSIONS

We have shown that the magnetostriction of field-structured magnetoelastomers is highly dependent upon the structure of the particle agglomerates. In increasing order of response are biaxial composites, random composites, uniaxial composites, and triaxial composites formed by heterodyning with a field bias. Magnetostrictions of up to 10 000 ppm have been demonstrated, as have modulus enhancements of 2000 kPa. We have shown that even for high aspect ratio samples demagnetizing field corrections can be important, and have identified a torque instability in some samples formed in biaxial fields. Finally, we have shown that there is a possibility of particle clumping transitions in these composites, and have shown how this transition depends on field, gel modulus, and sample strain. A future challenge is to understand precisely why the observed sample contraction increases linearly with sample preload.

ACKNOWLEDGMENTS

Sandia is a multiprogram laboratory operated by Sandia Corporation, a Lockheed Martin Company, for the United States Department of Energy under Contract No. DE-AC04-94AL8500. This work supported by the Division of Materials Science, Office of Basic Energy Sciences, U.S. Department of Energy (DOE).

[1] M. R. Jolly, J. D. Carlson, B. C. Munoz, and T. A. Bullions, J. Intell. Mater. Syst. Struct. **7**, 613 (1996).
[2] J. D. Carlson and M. R. Jolly, Mechatronics **10**, 555 (2000).
[3] J. Ginder, S. Clark, W. Sclhotter, and M. Nichols, Int. J. Mod. Phys. B **16**, 2412 (2002).
[4] G. Bossis, E. Coquelle, and P. Kuzhir, *Annales de Chimie* (Science des Materiaux); Nov.-Dec. 2004; Vol. 29, No. 6, pp. 43–54.

[5] J. E. Martin, R. A. Anderson, and R. L. Williamson, J. Chem. Phys. **118**, 1557 (2003).
[6] J. E. Martin, E. Venturini, J. Odinek, and R. A. Anderson, Phys. Rev. E **61**, 2818 (2000).
[7] J. E. Martin, E. Venturini, G. L. Gulley, and J. Williamson, Phys. Rev. E **69**, 021508 (2004).
[8] J. E. Martin and R. A. Anderson, J. Chem. Phys. **111**, 4273 (1999). This paper is written in the language of electrostriction, an isomorphic problem.
[9] J. A. Osborn, Phys. Rev. **67**, 351 (1946).
[10] Shape effect can be minimized by using elongated samples, incorporating the sample into a close-fitting solenoid, using the material to complete a reluctance circuit, etc.
[11] Divide by 4π to convert cgs or Gaussian units.